Please cite the Published Version

Enquiries:
If you have questions about this document, contact openresearch@mmu.ac.uk. Please include the URL of the record in e-space. If you believe that your, or a third party's rights have been compromised through this document please see our Take Down policy (available from https://www.mmu.ac.uk/library/using-the-library/policies-and-guidelines)

Industrial scale 3D printed catalytic converter for emissions control in a dual-fuel heavy-duty engine

Saeed Hajimirzaee[1], David Shaw[1], Paul Howard[2], Aidan M. Doyle[1*]

[1]Department of Natural Sciences, Manchester Metropolitan University, Chester Street, Manchester M1 5GD, United Kingdom

[2]G-Volution Ltd., Trym Lodge, Henbury Road, Bristol, BS9 3HQ, United Kingdom

[*]corresponding author: a.m.doyle@mmu.ac.uk

Abstract

A full size ceramic substrate was successfully prepared using a robocasting 3D printer and tested as a methane oxidation catalyst in the after treatment system (ATS) of a heavy-duty diesel engine, converted to co-combust (dual fuel) with natural gas (NG). The 3D printed substrate performance exceeded that of a commercially sourced straight-channelled DOC over most working conditions, despite the 3D printed structure having a lower precious group metal (PGM) loading and channels per square inch (CPSI) density. At moderate and high inlet temperatures, where the reaction rate is limited by internal and external mass transfer, the enhanced catalytic activity of the 3D printed substrate is attributed to the generation of internal turbulence, which increases oxidation rates of methane (CH_4) and non-methane hydrocarbons (NMHC). In contrast, there is relatively little difference between the catalytic activity of the 3D and straight-channelled substrates at low temperatures (e.g. cold start up), where the reaction is kinetically controlled and the additional turbulence/mass transfer of the 3D printed complex structure did not measurably alter the catalytic converter performance. Computational fluid dynamics (CFD) confirmed the increased turbulence within the channels of the 3D printed structure. We also report the effects of NG substitution on the fuel combustion efficiency under different engine load settings. The findings provide proof of concept evidence that 3D printing is a suitable means of designing a catalytic converter prototype with higher reaction activity than a conventionally extruded structure. This has significant implications for the design and potential mass production of new catalytic converters with enhanced efficiencies.

Keywords: dual fuel, after treatment system, diesel-natural gas engine, 3D print, additive manufacturing

1. Introduction

The transport sector is a major contributor to environmental pollution and climate change. According to the European Environment Agency, among 28 European countries in 2017, 27% of the total greenhouse gas emissions (including carbon dioxide, CO_2; methane, CH_4; and nitrogen oxides) came from the transport sector [1]. Despite significant increases in the number of motor vehicles, current technologies are still not sufficiently advanced to fully alleviate the toxic effects of emissions. This problem is most evident in the populated areas of cities in developing countries where overcoming urban air pollution is considered one of the main goals in improving public health [2].

Heavy-duty diesel engines are at the heart of the transportation of goods. High durability and reliability, long service life, low maintenance and high torque output make these engines the first choice for such applications. Many buses, heavy trucks, tractors, locomotives, ships, marine barges, tugboats and generators use heavy-duty diesel engines. Harmful exhaust emissions from these engines, especially particulate matter (PM) and NO_x are responsible for several health problems [3, 4]. Dual-fuel engines employing diesel-LNG [5, 6], diesel-LPG [7, 8], diesel-CNG [9, 10] and diesel-alcohol [11, 12] combinations have been widely studied as a promising approach to lower the dependence on petroleum based liquid fuels as well as reducing the emissions of CO_2, PM and NO_x [13]. The choice of which alternative fuel to use is examined in terms of availability, source, storage, safety, toxicity, health emission and engine performance. Natural gas (NG) is a promising secondary fuel for duel fuel engines as it can meet most of the mentioned criteria. Its advantages over diesel are much higher abundance, lower price, lower carbon (overall) and NO_x emissions, higher octane number, and better mixing with air to give a more uniform temperature distribution and higher thermal energy output [13, 14]. However, dual-fuel engines produce higher emissions of CO than diesel only and also emit unburnt methane (known as methane slip): overcoming these drawbacks is the main obstacle to the rollout of dual fuel systems in the heavy-duty transportation and power generation sector..
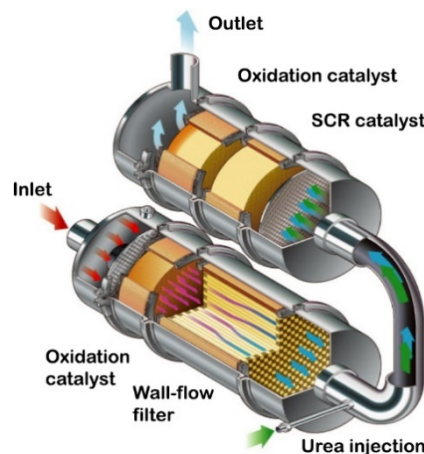

Figure 1. Johnson Matthey SCRT® (Selective Catalytic Reduction Technology) system for emission control in heavy-duty diesel engines [15].

The implementation of the Euro I regulation by the European Commission in 1993, and progressively more stringent emissions limits since e.g. Euro VI, made the after treatment emission control systems (ATS) the only realistic solution to decrease emissions. A typical ATS consists of a diesel particulate filter (DPF), diesel oxidation catalyst (DOC), and selective catalytic reduction (SCR) (Figure 1). In the auto industry, the common catalyst support for a DOC is a monolith honeycomb cordierite ($2MgO.2Al_2O_3.5SiO_2$) substrate coated with a platinum metal group (PMG) catalyst and canned within a stainless-steel container [16]. The properties of DOCs are defined based on different parameters including light-off temperature, efficiency in elimination of CO and hydrocarbons, thermal stability, resistance against poisoning and cost. These properties mainly depend on the monolith structure e.g. channels per square inch (CPSI), wall thickness, the converter external dimensions (cross-sectional area and length) and amount of PGM washcoated on the substrate and total exhaust gas flow rate or space velocity.

The CPSI and wall thickness determine the heat up response, back pressure, and mechanical stability of the catalytic converter [2]. The CPSI of ceramic substrates for automotive catalytic converter applications is in the range 400-900 with wall thickness of 0.004 in (0.1 mm) [17]. Recently, ceramic substrates with 900-1200 CPSI and 0.002 in (0.05 mm) wall thickness have been manufactured and shown promising results in conversion efficiency and production costs but had shorter life time and low mechanical stability [18]. The current commonest substrate for heavy-duty diesel engines has CPSI in the range of 300-400. It is well know that the flow regime inside the channels is laminar and, therefore, the reactants must diffuse radially toward the washcoat. Analogously, heat transfer from the washcoat to the bulk gas phase mainly occurs by radial conduction [19]. At low temperatures (e.g. temperatures less than light-off), the reaction rate is kinetically controlled while at post light-off temperatures, the conversion depends on the mass transfer coefficient, which is a function of external and internal mass transfer. For typical vehicle drive cycles, the catalyst mostly operates in the mass transfer regime; therefore, the heat and mass transfer rates in a monolith with straight channels are limited to radial diffusion and conduction [20].

It has been shown that introducing turbulence, either before the substrate or inside the channels, can significantly improve the conversion efficiency of the catalytic converter at the penalty of backpressure. Utilisation of a swirl blade configuration before the monolith [21, 22] has shown promising results with slight improvement in catalytic converter efficiency. Employing corrugated metallic foils with internal holes [23, 24] is another approach, however the cost of metallic substrates and complexity of wash coating are the main concerns associated with this class of substrates [25].

In 3D printing, a material is prepared point-by-point, line-by-line or layer-by-layer in an additive manner by means of sliced (using software) 2D cross sections from a 3D Computer Aided Design (CAD) model. 3D printing, thus, enables the preparation of highly complex and precise structures that are difficult, or impossible, to make using traditional methods e.g. extrusion, casting or machining [26]. The 3D printing of ceramic material for catalytic applications has attracted interest from both academia and industry. Examples include 3D printed substrates for CO_2 removal [27, 28], conversion of methanol to olefins [29, 30], cracking of alkanes to light olefins [31] and production of pharmaceutical agents [32, 33].

We recently reported the successful use of 3D printing in the preparation of miniature (up to 5 cm diameter) model substrates with enhanced structures in the low temperature catalytic oxidation of methane at lab scale [34]. Here, we demonstrate for the first time the preparation of a 3D printed industrial scale catalytic converter and its application in the ATS of a dual fuel heavy-duty engine over a range of realistic working conditions.

2. Experimental

2.1 Substrate 3D printing

Commercial porcelain (white Earthenware porcelain, WASP, Italy), in paste form, was mixed with water and ethylene glycol with volumetric ratio of 1:2 and kneaded until the rheology became suitable for 3D printing. Four equally sized circular sector quadrants were printed using a WASP 4070 ceramic 3D printer with nozzle diameter of 700 μm to produce a substrate with overall dimensions Ø320 mm x H120 mm (including 20% overall dimension scale up to compensate for shrinkage after drying and sintering). The CAD design was

prepared using SketchUp 2018 and converted to g-code using Cura v3.5. The fabrication method is based on the Liquid Deposition Modelling (LDM) or Robocasting (RC) technique in which the substrate is made through layer-by-layer deposition of ceramic paste and built from bottom to top. 3D printed samples were dried at room temperature for 48 h followed by sintering at 1200 ºC (1 °C/min) for 8 h.

2.2 Catalytic converter preparation

The catalyst washcoat was prepared according to the following procedure:

Support suspension: 80 g of support powder was prepared by mixing HY Zeolite (CBV 760, Zeolyst International), γ-Al_2O_3 (Sigma-Aldrich, activated, neutral), TiO_2 (Millennium PC500), CeO_2 (Sigma-Aldrich, Nano-powder <25nm particle size), and ZrO_2 (Sigma-Aldrich, 5µm, 99%) with mass ratio 12:3:3:1:1, respectively. 1000 ml of water was added to the solid powder and stirred, and the pH was adjusted to 11 by adding NH_4OH solution.

Precious metal solution: 19.89 g $Pd(NO_3)_2.H_2O$ (Alfa Aesar, 99.8%) and 7.13 g K_2PtCl_4 (Precious Metals Online, 99%) were dissolved in distilled water in two separate 500 ml volumetric flasks, followed by ultrasonic treatment for 15 min. Precious metal solution was added dropwise to the support suspension, stirred for 2 hours followed by ultrasonic treatment for 15 min. The resulting suspension was applied as a washcoat to the 3D printed substrate using an air-pressurised spray gun, followed by drying at 50 ºC for 24 h and calcination at 550 ºC for 8 h. The commercial DOC was part of an OEM standard aftertreatment package used by MAN on their 10.5l D2086 EU6 engine.

2.3 Substrate testing

The 3D printed catalytic converter performance was assessed at Helical Technology ltd. using a Euro 6 MAN D2086 10.5 L, 265 kW diesel-natural gas engine attached to a commercial dyno (Oswald AC Motor Dyno, 601 kW). The exhaust gas composition was analysed using a Horiba Mexa 7170 DEGR emissions analyser. A series of experiments were conducted with different engine load and diesel substitution with CNG to cover a range of ATS inlet temperatures, gas hour space velocities (GHSV) and gas compositions. Table 1 lists the test points with different operating conditions for both 3D printed and commercial substrates. The engine speed for all the tests points was kept constant at 1200 rpm and the load (torque) was normalised (0-100%) as a function of the maximum 1800Nm available at this speed. The slight differences in ATS inlet temperatures and GHSV for the two substrates is because of differences in actual gas and diesel mass flow rates into the engine due to external variables. Figure 2 shows the actual mass flow rate of diesel and NG at different loads for the 3D printed and commercial substrates. Exact values for some points have been shown as examples. In both cases, higher loads required the diesel and NG flow rates to increase non-linearly to keep the engine speed fixed at 1200 rpm. For instance, in experiments with the commercial DOC using 20% NG substitution at lowest load, the diesel flow rate decreased from 7.1 to 5.6 kg/h (21% decrease), while at full load, this decrease was from 44.5 to 32.3 kg/h (27% decrease).

Table 1. Test point conditions with different GHSVs and temperatures used for evaluation of 3D printed and commercial DOC.

| Test Point	Load (%)	Nominal NG substitution	Actual NG substitution	3D printed		Commercial	
				ATS inlet T (ºC)	GHSV (1/h)	ATS inlet T (ºC)	GHSV (1/h)
1	3	40	41	165	20,000	169	16,700
2	3	30	28	164	20,000	165	17,100
3	3	20	22	164	19,900	161	17,500
4	3	0	0	159	19,600	150	21,400
5	25	40	41	259	30,300	247	31,300
6	25	30	35	256	29,700	245	29,800
7	25	20	24	254	29,100	243	28,000
8	25	0	0	248	28,600	248	32,700
9	42	40	37	308	42,500	308	47,500
10	42	30	29	306	42,000	307	46,900
11	42	20	20	304	42,300	304	46,200
12	42	0	0	298	42,700	298	46,100
13	83	40	35	354	79,000	349	86,200
14	83	30	27	354	80,000	349	86,200
15	83	20	21	354	79,200	349	83,600
16	83	0	0	347	79,500	347	87,100
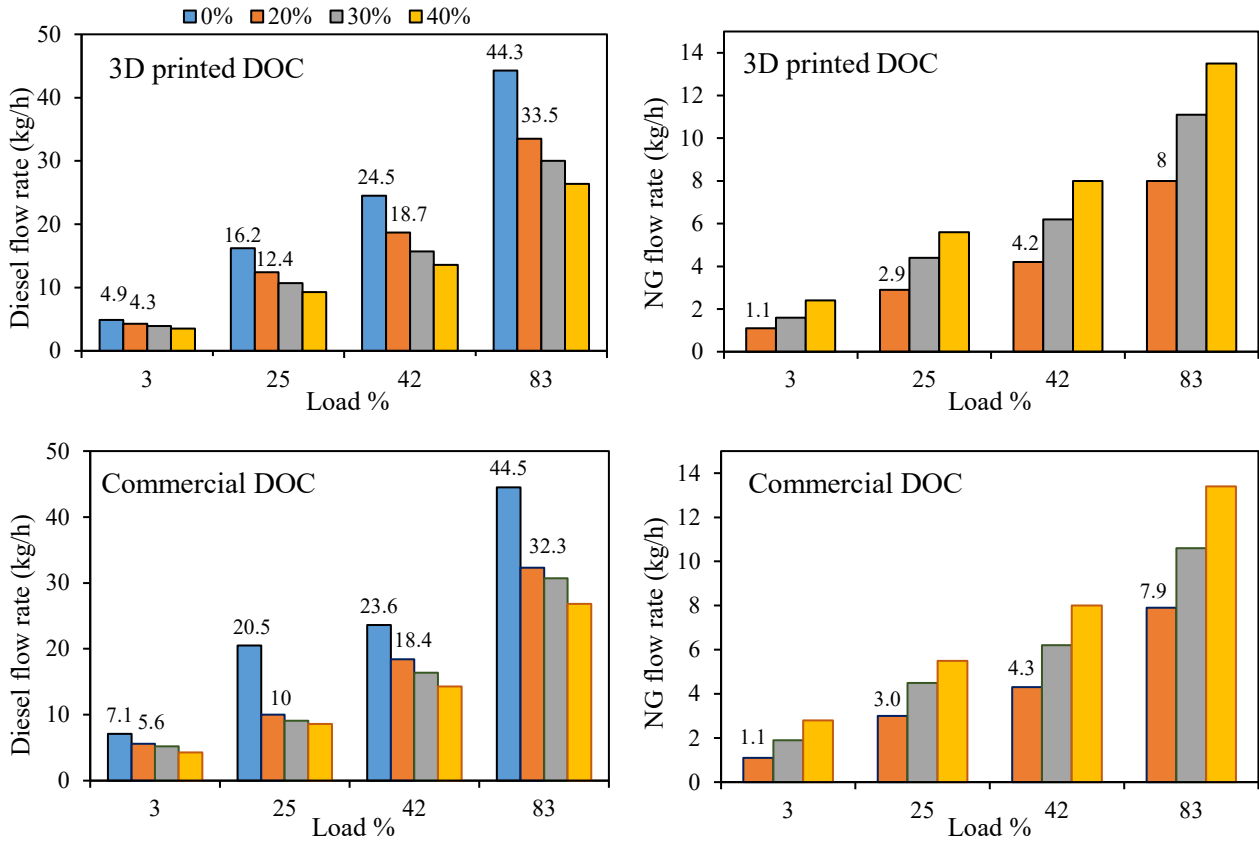
Figure 2. Diesel and NG mass flow rate at different loads and NG substitutions using 3D printed and commercial DOC.

Net indicated efficiency (NIE) and fuel combustion efficiency are parameters that have been used in this study to evaluate the engine performance at different working conditions. NIE is based on net work done on the piston over the full engine cycle and includes work used to overcome friction and accessory loads. These parameters were calculated using the equations proposed by Pedrozo et al. [35] for dual fuel engines:

$$Net\ Indicated\ Efficiency\ (\%) = \frac{3600\ P_{ind}}{\dot{m}_{diesel} \times LHV_{diesel} + \dot{m}_{gas} \times LHV_{gas}} \times 100$$

where P_{ind} is the net indicated power in kW, $\dot{m}$ is the mass flow rate of fuel in kg/h, LHV is the lower heating value of fuel in kJ/kg.

$$Combustion\ Efficiency\ (\%) = \left(1 - P_{ind} \times \left[\frac{IS_{CO} \times LHV_{CO} + IS_{THC} \times LHV_{DF}}{\dot{m}_{diesel} \times LHV_{diesel} + \dot{m}_{gas} \times LHV_{gas}}\right]\right) \times 100$$

where IS_{CO} and IS_{THC} are the net indicated specific emissions of CO and total hydrocarbons in kg/kWh and calculated as the ratio of emission mass flow rate to P_{ind}; LHV_{CO} is equivalent to 10100 kJ/kg; and LHV_{DF} is the actual lower heating value of dual fuel in the cylinder given by:

$$LHV_{DF} = \frac{\dot{m}_{diesel} \times LHV_{diesel} + \dot{m}_{gas} \times LHV_{gas}}{\dot{m}_{diesel} + \dot{m}_{gas}}$$

Conversions of CH_4, CO and NMHC were calculated according to the following equation:

$$Methane\ conversion(\%) = \frac{[CH_4]_{in} - [CH_4]_{out}}{[CH_4]_{in}}$$

where concentrations are in ppm.

2.4 CFD modelling

CFD analysis was performed using ANSYS Fluent v19.1 platform. The domain was built using the approach adapted from a sub-grid scale modelling consisting of a cylindrical element, Ø 10mm x L 100mm, instead of considering the whole structure. A 100 mm cylindrical space before and after the substrate was allocated for uniform flow dispersion. The geometry was imported to Design Modeler and introduced to the Ansys meshing component. The fluid domain and solid substrate was meshed using the Hybrid method (hexahedral-tetrahedral) which is constituted by 1,314,607 and 2,897,693 cells for the 3D printed and commercial DOCs, respectively (Figure 3).
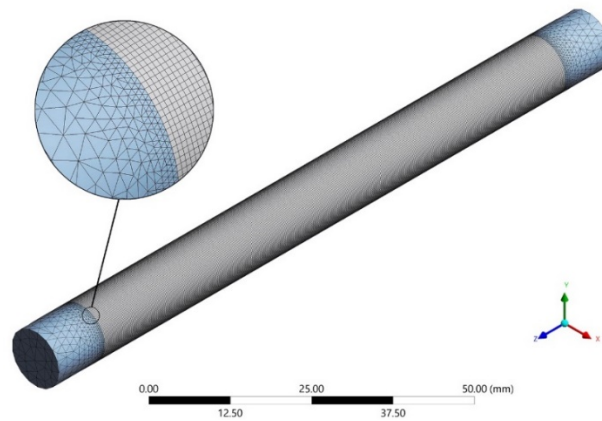

Figure 3. Fluid domain mesh for CFD analysis.

The typical boundary conditions are as follow: inlet velocity 0.626 m/s, k (turbulent kinetic energy) 0.0015 m^2/s^2, I (initial turbulence intensity) 0.05%, ε (turbulence dissipation rate) 0.0005 m^2/s^3, the outlet pressure was set to atmospheric pressure and the wall was defined as a no slip condition at the fixed temperature of 250 °C (523 K). Equations to calculate k and ε are as follows [36]:

$$k = \frac{3}{2}(u_{avg}I)^2 \qquad I = 0.16Re^{-\frac{1}{8}} \qquad \varepsilon = \frac{C_u^{\frac{3}{4}}k^{\frac{3}{2}}}{l} \qquad l = 0.07L$$

where C_u is an empirical constant, approximately 0.09, specified in the turbulence model, and L is the characteristic length, which is the diameter of the catalytic converter in this case. Realizable k-epsilon turbulence with default constants ($C_{2\varepsilon}$=1.2, TKE Prandtl Number = 1.0, TDR Prandtl Number = 1.2) under steady state conditions were used for the viscous model. Air at 250 °C and atmospheric pressure was used as the inlet fluid.

3. Results and discussion

3.1 Substrate preparation

Figure 4 shows the CAD designs of the 3D lattice structure and compares its cross-sectional structure with the conventionally extruded honeycomb monolith. The structure consists of layers, which are rotated at an offset angle of 90º to the previous layer. Each layer is made of an array of parallel rods, which are separated by 1 mm distance, resulting in a cylindrical woodpile structure with a lattice of orthogonally interconnected rods. The CAD design was divided into 4 equal sub-sections and used in slicing software to generate the g-code for 3D printing.
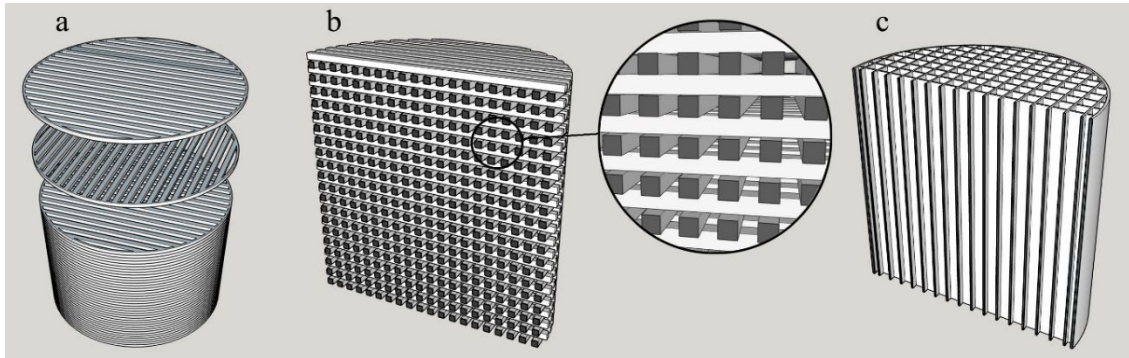

Figure 4. a) 3D printed structure consists of rotated layers, b) cross-sectional view of 3D printed substrate with 90° layer rotation, c) cross-sectional view of conventional structure with straight channels (CPSI 400).

The catalytic converter was assembled by canning the washcoated quadrants, using the stuffing method, and securing in place by means of a support mat make-up of ceramic fibre (Figure 5). Stuffing is a canning method where the substrate is covered by a support mat and then pushed into a metallic body (mostly stainless steel), using a stuffing cone. The stuffing cone is used to compress the support mat and manage the radial forces exerted on the substrate during insertion to the sleeve (manufacturing); the role of the mat is to ensure adequate holding force is applied to the substrate whilst accommodating the differential in thermal expansion between the substrate and sleeve. [37]

Figure 5. 3D printed substrate washcoated and canned for testing as DOC.

The specifications of the 3D printed and commercial DOCs are listed in Table 2. The 3D printed substrate has lower CPSI than the commercial sample, 100 versus 400, which was due to the limitation in how thin the rods could be prepared using this 3D printing method. The main difficulty was the partial blockage of the nozzle caused by extrusion of the highly viscous ceramic paste through an opening with diameter less than 0.7 mm. However, repeated attempts incorporating iterative refinements in ceramic paste and printing method resulted in successful and reliable prints. The amount of PGM in the 3D printed DOC, 2.2 g/L, was less than the commercial sample, 2.6 g/L. An SEM image of the catalyst before washcoating (Figure 6) confirms the characteristic zeolite Y particle structure, which is consistent with our previous report using a similar washcoat catalyst preparation [34].

Table 2. Specifications of catalytic converters after sintering and washcoat.

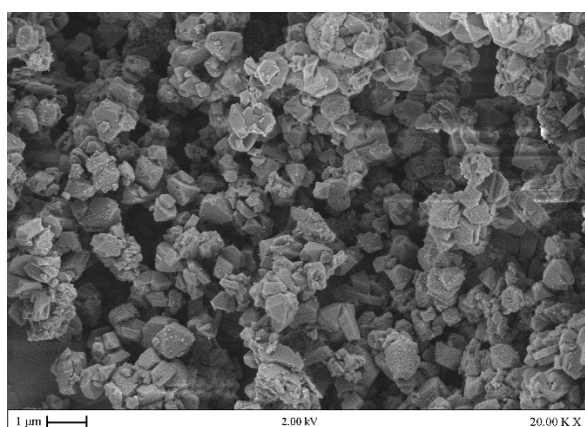| Substrate	3D printed DOC	Commercial DOC
CPSI	100	400
Diameter (mm)	266.7	266.7
Height (mm)	101.6	101.6
Volume of substrate (L)	5.7	5.7
Total Pd content (g)	9.15	7.5
Total Pt content (g)	3.35	7.5
PGM loading (g/L)	2.2	2.6

Figure 6 SEM imaging of catalyst washcoat.

3.2 Fuel combustion properties

While the main topic in this paper focuses on the benefits of 3D printed substrates in decreasing dual-fuel engine exhaust emissions, we include here additional data, for information purposes, showing the fuel combustion efficiencies for the same operating conditions as those employed in the subsequent section on emissions. Table 3 lists the calculated values for net indicated efficiency (NIE) at different loads and NG substitutions. It is well known that at low loads, NIE and brake efficiency are severely affected due to pumping and friction losses. Friction loss not only includes mechanical friction of the engine but also the energy that is used to drive the high pressure fuel pump at low loads [38]. Increasing the load from 3% to full caused the NIE to increase proportionally. However, this increase is higher when more gas is substituted. For instance, using diesel only, the increase in NIE from low load to full load is 179%, while at 40% substitution, this increase is 272%. Therefore, NIE, as an indicator to show how much energy is converted to work, reveals another benefit from dual fuelling, especially at high substitution rates.

Table 3. Net indicated efficiency at different load and NG substitution

NG substitution (%)	NIE at different loads*				Change from 3%-83% load
	3%	25%	42%	83%	
0	12.8	29.3	32.3	35.7	+179%
20	11.5	30.6	34.1	37.6	+227%
30	11.2	30.8	35.4	37.8	+238%
40	10.4	31.0	35.7	38.7	+272%

* LHV_{Diesel} = 42910 kJ/kg; LHVgas = 45860 kJ/kg

Figure 7 illustrates the fuel combustion efficiency for different NG substitutions and loads on the testing runs with the 3D printed DOC. (The trends for the experiments with the commercial substrate were similar so are not shown here.) Using diesel only, the diesel combustion efficiency is >99.9% at the different loads; however there is a noticeable decrease in fuel combustion efficiency when it is substituted by NG, especially at low load. For instance at 3% load, when 20, 30 and 40% of diesel is substituted, the fuel combustion efficiency is decreased to 95.4, 93.5 and 89.9%, respectively. The combustion efficiency increases with increasing load, where the engine is working at progressively higher temperatures and pressures; for example, at full load the combustion efficiency is >99.5% over all NG substitutions.
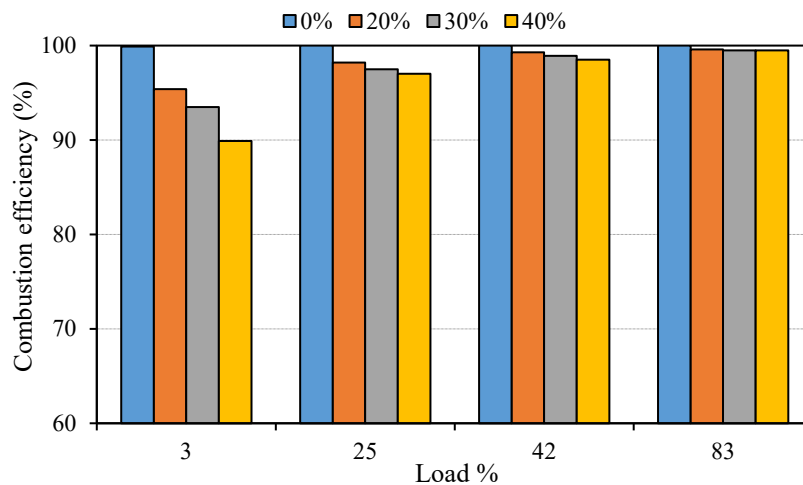
Figure 7. Engine combustion efficiency as a function of NG substitution and load % over 3D printed DOC.

3.3 Catalytic activity

The catalytic activity of the 3D printed DOC in emissions abatement (e.g. conversion of CO, CH_4 and other heavier hydrocarbons) was compared with that of a commercial DOC over a range of operating conditions. The results are presented in Table 4. At low temperatures, i.e. below 200ºC, which are points 1-4, conversion is generally lower on the 3D printed substrate. For instance, at test point 1, where 40% of diesel was substituted by NG, CO conversion is only 33% on 3D printed substrate, while it is 54% for the commercial DOC. Similarly, CH_4 conversion and NMHC conversions are 21% and 24%, respectively, for the 3D printed DOC, while these values are around 35% for the commercial DOC. This means that, in most cases, at lower temperature the commercial DOC is performing better than the 3D printed. At these low temperatures, the reaction is kinetically controlled, where the reaction rate is limited by the chemical kinetics of the oxidation reaction; any additional turbulence that increases mass transfer rates over the 3D printed DOC, therefore, has a relatively insignificant effect on the overall oxidation rate (at least for the conditions studied here). In this region, the catalyst temperature is essentially the same as the bulk stream temperature [39]. Therefore, the higher conversion on the commercial DOC can be attributed to the higher PGM loading on the washcoat or its special formulation (e.g. optimised Pd to Pt ratio or employing other promoters to kinetically enhance the reaction over the catalyst surface). It should be noted that under diesel only conditions, CH_4 was not detected in the engine out stream.

Table 4. Conversion% of CO, CH_4 and NMHC over 3D printed and commercial substrates.

Test Point	Nominal NG substitution	3D printed DOC			Commercial DOC		
		CO	CH_4	NMHC	CO	CH_4	NMHC
1	40	33	21	24	54	35	36
2	30	53	11	18	68	40	42
3	20	100	18	31	82	22	53
4	0	100	--	100	100	--	93
5	40	100	31	45	100	24	38
6	30	100	34	51	100	30	56
7	20	100	42	61	100	33	60
8	0	100	--	100	98	--	97

10

9	40	100	31	52	100	22	50
10	30	100	27	54	100	27	55
11	20	100	29	64	100	31	69
12	0	100	--	100	100	--	99
13	40	100	36	71	100	36	76
14	30	100	37	74	100	36	78
15	20	100	37	82	100	35	83
16	0	100	--	100	100	--	100

At higher temperatures (e.g. point 5-16), where the temperature is in the range 200-300 ºC, the conversions of CH_4 and NMHC are higher on the 3D printed substrate. For instance, under the operating conditions at point 5, CH_4 and NMHC conversions are 31% and 45% over the 3D printed substrate, while these values are 24% and 38% for the commercial DOC, respectively. At higher temperatures, the oxidation reaction rate increases to a greater extent than those of the external and internal mass transfer rates. Therefore, the main resistance is due to external and internal mass transfer such that the reaction rate is mass transfer limited. In this region, the additional reaction rate causes the catalyst surface temperature to be much higher than the bulk gas stream, which further increases the reaction rate [40-42]. Similarly, for other points, a better conversion efficiency was observed over the 3D printed substrate, especially under conditions where 40% of diesel was substituted with NG (e.g. points 5, 9 and 13). In commercial automotive catalytic converters, the reduced overall conversion in the first few minutes after cold start-up of the engine is a threat for licensing the devices, because the latest legislative test cycles cover this temperature range [43].

Overall, the emissions activities clearly support the application of 3D printing to prepare catalytic converters with channel complexities superior to those using conventional extrusion. Furthermore, the findings here are particularly promising when one considers that that the CPSI for the commercial substrate (400) is 4 times higher than that for the 3D printed substrate (100) and uses a catalyst with a higher PGM loading.

3.4 CFD analysis

Figure 8 compares the velocity magnitude over the commercial and 3D printed substrates. Obviously, the maximum velocity is in the centre of the channels and is lower near the walls; however, this maximum velocity is much higher on the 3D printed substrate than the commercial straight channelled structure. The cross-sectional view suggests that the velocity profiles inside the channels of the 3D printed substrate can be classified into four regions; velocity in the range 0.3-0.7 m/s (cyan colour); 0.8-1.6 m/s (green colour); 1.7-1.9 m/s (yellow colour): and 2.0-2.7 m/s (orange colour), while the velocity profiles in the conventional monolith structure are divided into two groups: velocity in the range 0.3-0.8 m/s (cyan colour) and velocity in the range 0.9-1.5 m/s (green colour). Figure 9 illustrates the turbulent kinetic energy within the channels. Generally, the 3D printed structure shows a higher degree of turbulence in the channels, which is higher in regions close to the walls where the interconnection between rotated walls exists. This introduces internal turbulence in the channels, while most of the flow through the straight line channels has much lower turbulent kinetic energy (e.g. less than 0.08 m^2/s^2) which are shown in dark blue colour. Therefore, we assign the higher conversion efficiencies of the 3D printed substrate to the turbulence induced by the interconnected walls, despite the CPSI being lower than the commercial substrate.
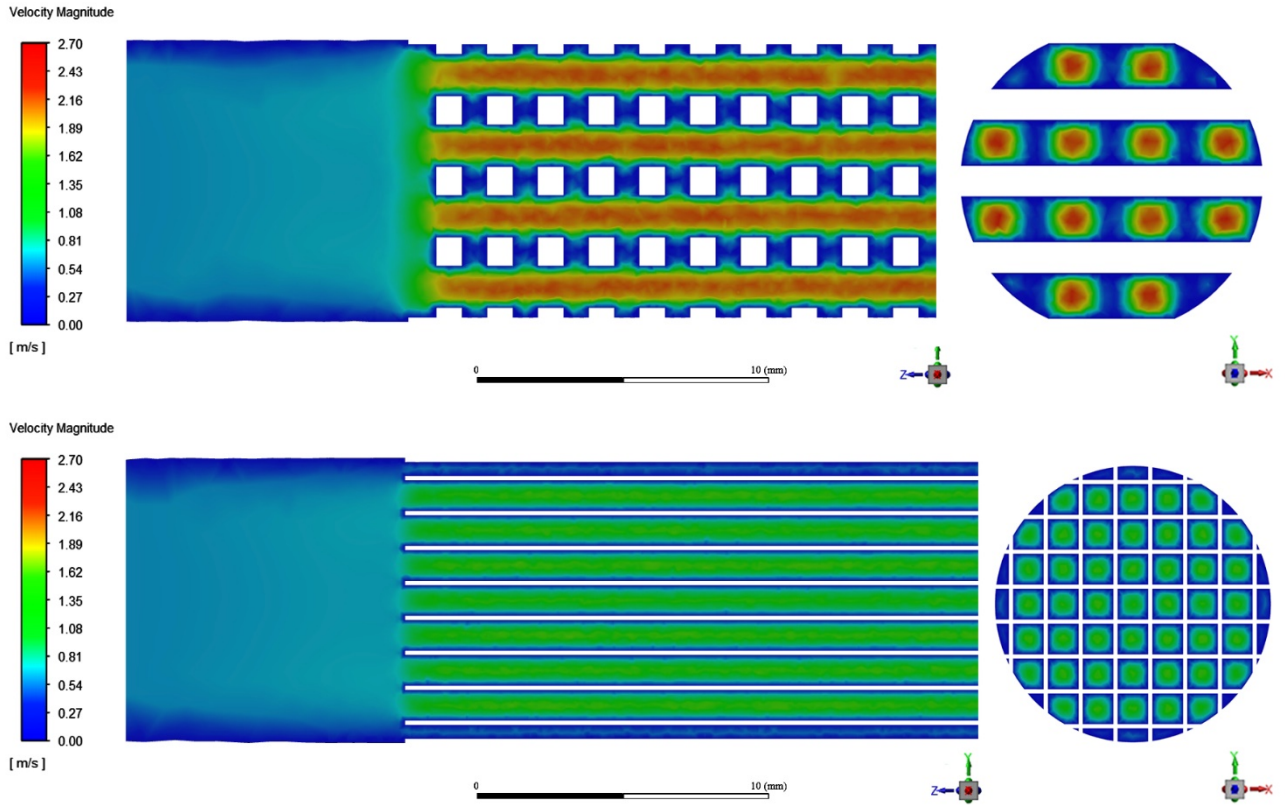
Figure 8. Velocity magnitude profile along flow direction and cross section at the entrance for 3D printed substrate (top) and commercial substrate (bottom).
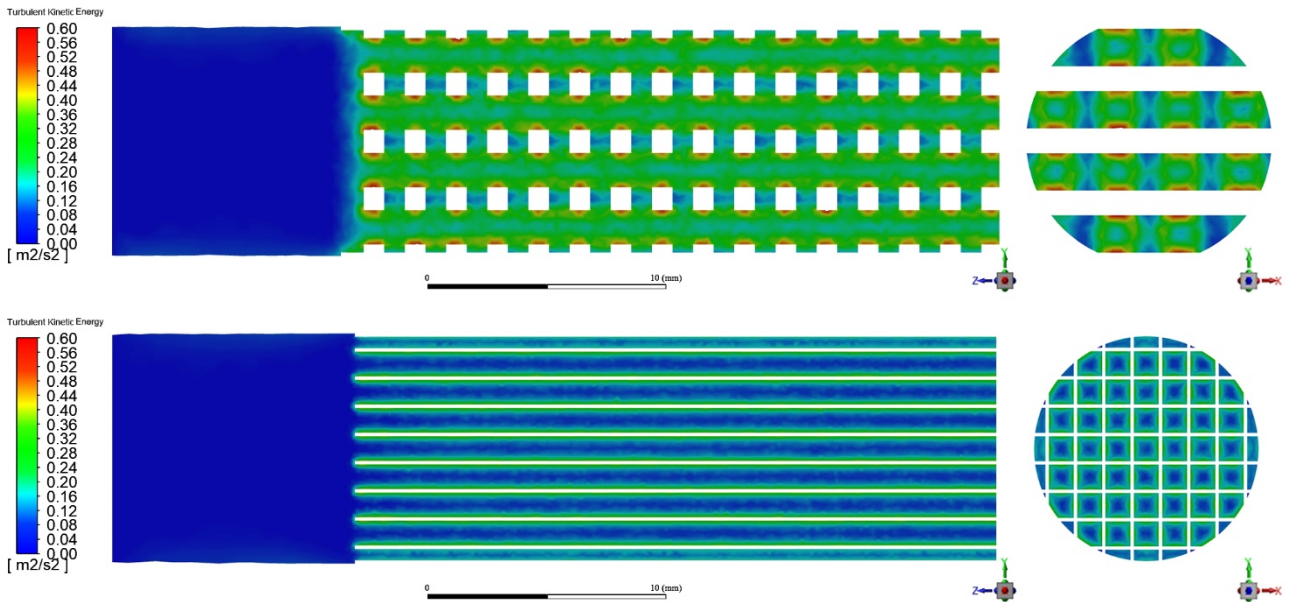

Figure 9. Turbulent kinetic energy along flow direction and cross section at the entrance for 3D printed substrate (top) and commercial substrate (bottom).

Figure 10 shows the static pressure gradient across the two structures. An overall pressure drop around 65 Pa was observed over the 3D printed structure and was 50 Pa for the commercial structure. The higher pressure

drop on the 3D printed substrate is attributed to the induced turbulence caused by the 3-dimensionally oriented channel arrangement.
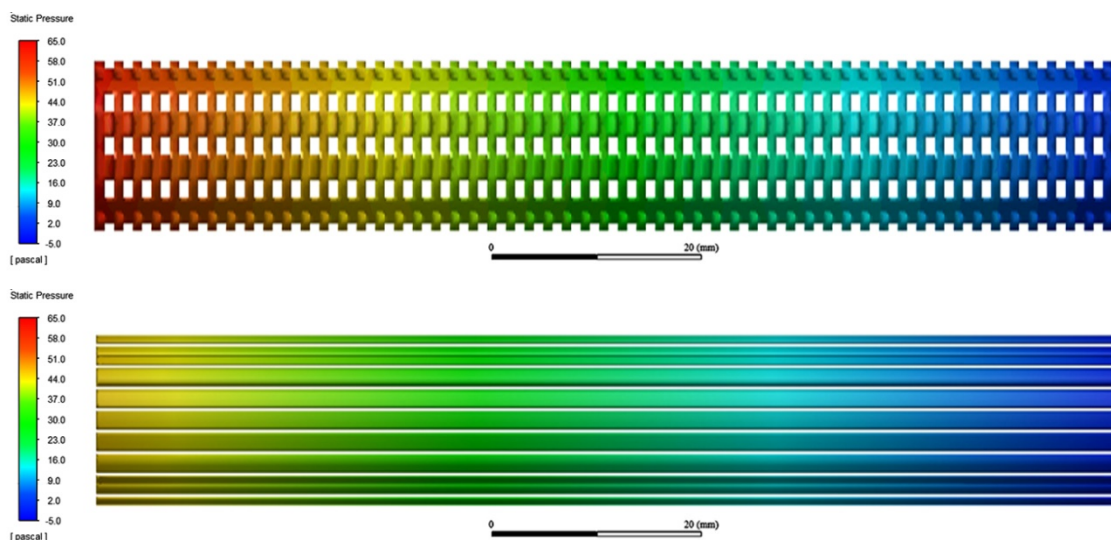

Figure 10. Overall static pressure profile along flow direction for 3D printed substrate (top) and commercial substrate (bottom). Flow inlet from left.

4. Conclusions

A DOC catalytic converter prepared by 3D printing of ceramic showed improved catalytic activity in conversion of CO, methane and NMHC in a dual-fuel heavy-duty diesel engine, relative to a conventional honeycomb structure with straight channels. It was shown that the 3D structure induced internal turbulence, which increased conversion at moderate and high temperatures where the reaction rate was governed by internal and external mass transfer. The results show that 3D printing is a viable method to design and prepare catalytic converter structures whose properties exceed those that are commercially available.

5. Acknowledgements

6. References

[1] EEA. Greenhouse gas emissions from transport in Europe. Copenhagen, Denmark: European Environment Agency; 2019.

[2] Reşitoğlu İA, Altinişik K, Keskin A. The pollutant emissions from diesel-engine vehicles and exhaust aftertreatment systems. Clean Technologies and Environmental Policy 2015;17(1):15-27.

[3] Zheng M, Reader GT, Hawley JG. Diesel engine exhaust gas recirculation—a review on advanced and novel concepts. Energy Conversion and Management 2004;45(6):883-900.

[4] Fiebig M, Wiartalla A, Holderbaum B, Kiesow S. Particulate emissions from diesel engines: correlation between engine technology and emissions. Journal of Occupational Medicine and Toxicology 2014;9(1):6.

[5] Cheenkachorn K, Poompipatpong C, Ho CG. Performance and emissions of a heavy-duty diesel engine fuelled with diesel and LNG (liquid natural gas). Energy 2013;53:52-7.

[6] Kumar S, Kwon H-T, Choi K-H, Lim W, Cho JH, Tak K, et al. LNG: An eco-friendly cryogenic fuel for sustainable development. Applied Energy 2011;88(12):4264-73.

[7] Saleh HE. Effect of variation in LPG composition on emissions and performance in a dual fuel diesel engine. Fuel 2008;87(13-14):3031-9.

[8] Lata DB, Misra A, Medhekar S. Investigations on the combustion parameters of a dual fuel diesel engine with hydrogen and LPG as secondary fuels. International Journal of Hydrogen Energy 2011;36(21):13808-19.

[9] Liu J, Yang F, Wang H, Ouyang M, Hao S. Effects of pilot fuel quantity on the emissions characteristics of a CNG/diesel dual fuel engine with optimized pilot injection timing. Applied Energy 2013;110:201-6.

[10] Nithyanandan K, Lin YL, Donahue R, Meng XY, Zhang JX, Lee CFF. Characterization of soot from diesel-CNG dual-fuel combustion in a CI engine. Fuel 2016;184:145-52.

[11] Campos-Fernández J, Arnal JM, Gómez J, Dorado MP. A comparison of performance of higher alcohols/diesel fuel blends in a diesel engine. Applied Energy 2012;95:267-75.

[12] Xing-cai L, Jian-guang Y, Wu-gao Z, Zhen H. Effect of cetane number improver on heat release rate and emissions of high speed diesel engine fueled with ethanol–diesel blend fuel. Fuel 2004;83(14):2013-20.

[13] Ashok B, Denis Ashok S, Ramesh Kumar C. LPG diesel dual fuel engine – A critical review. Alexandria Engineering Journal 2015;54(2):105-26.

[14] Karagöz Y, Sandalcı T, Koylu UO, Dalkılıç AS, Wongwises S. Effect of the use of natural gas–diesel fuel mixture on performance, emissions, and combustion characteristics of a compression ignition engine. Advances in Mechanical Engineering 2016;8(4):1687814016643228.

[15] Matthey J. JM's SCRT® System for On-Road Vehicle NOx Reduction. *Global Emissions Management.* 3. Royston, UK: Johnson Matthey Plc; 2010.

[16] Ayodhya AS, Narayanappa KG. An overview of after-treatment systems for diesel engines. Environmental Science and Pollution Research 2018;25(35):35034-47.

[17] Williams JL. Monolith structures, materials, properties and uses. Catalysis Today 2001;69(1-4):3-9.

[18] Wiehl J, Vogt CD. Ceramic ultra-thin-wall substrates for modern catalysts. MTZ worldwide 2003;64(2):8-11.

[19] Schweich D, Leclerc JP. Flow, Heat, and Mass Transfer in a Monolithic Catalytic Converter. In: Crucq A, editor Studies in Surface Science and Catalysis. Elsevier; 1991, p. 437-63.

[20] Benjamin SF, Liu Z, Roberts CA. Automotive catalyst design for uniform conversion efficiency. Applied Mathematical Modelling 2004;28(6):559-72.

[21] Agrawal T, Banerjee VK, Sikarwar BS, Bhandwal M. Optimizing the Performance of Catalytic Convertor Using Turbulence Devices in the Exhaust System. In: Kumar M, Pandey RK, Kumar V, eds. *Advances in Interdisciplinary Engineering.* Singapore: Springer Singapore; 2019:333-42.

[22]   Bhandwal M, Kumar M, Sharma M, Srivastava U, Verma A, Tyagi RK. The effect of using the turbulence enhancement unit before the catalytic converter in diesel engine emissions. International Journal of Ambient Energy 2018;39(1):73-7.

[23]   Dawson EK, Kramer J. Faster is Better: The Effect of Internal Turbulence on DOC Efficiency. SAE International; 2006.

[24]   Rice M, Kramer J, Mueller-Haas K, Mueller R. Innovative Substrate Technology for High Performance Heavy Duty Truck SCR Catalyst Systems. SAE Technical Paper; 2007.

[25]   Govender S, Friedrich HB. Monoliths: a review of the basics, preparation methods and their relevance to oxidation. Catalysts 2017;7(2):62.

[26]   Gibson I, Rosen DW, Stucker B. Introduction and Basic Principles. In: Gibson I, Rosen DW, Stucker B, editors. Additive Manufacturing Technologies: Rapid Prototyping to Direct Digital Manufacturing. Boston, MA: Springer US; 2010, p. 20-35.

[27]   Couck S, Lefevere J, Mullens S, Protasova L, Meynen V, Desmet G, et al. CO_2, CH_4 and N_2 separation with a 3DFD-printed ZSM-5 monolith. Chemical Engineering Journal 2017;308:719-26.

[28]   Thakkar H, Eastman S, Hajari A, Rownaghi AA, Knox JC, Rezaei F. 3D-Printed Zeolite Monoliths for CO_2 Removal from Enclosed Environments. ACS Applied Materials & Interfaces 2016;8(41):27753-61.

[29]   Li X, Rezaei F, Rownaghi AA. 3D-printed zeolite monoliths with hierarchical porosity for selective methanol to light olefin reaction. Reaction Chemistry & Engineering 2018;3(5):733-46.

[30]   Magzoub F, Li X, Al-Darwish J, Rezaei F, Rownaghi AA. 3D-printed ZSM-5 monoliths with metal dopants for methanol conversion in the presence and absence of carbon dioxide. Applied Catalysis B: Environmental 2019;245:486-95.

[31]   Li X, Li W, Rezaei F, Rownaghi A. Catalytic cracking of n-hexane for producing light olefins on 3D-printed monoliths of MFI and FAU zeolites. Chemical Engineering Journal 2018;333:545-53.

[32]   Tubío CR, Azuaje J, Escalante L, Coelho A, Guitián F, Sotelo E, et al. 3D printing of a heterogeneous copper-based catalyst. J Catal 2016;334:110-5.

[33]   Azuaje J, Tubío CR, Escalante L, Gómez M, Guitián F, Coelho A, et al. An efficient and recyclable 3D printed α-Al_2O_3 catalyst for the multicomponent assembly of bioactive heterocycles. Applied Catalysis A: General 2017;530:203-10.

[34]   Hajimirzaee S, Doyle AM. 3D printed catalytic converters with enhanced activity for low-temperature methane oxidation in dual-fuel engines. Fuel 2020;274:117848.

[35]   Pedrozo VB, Zhao H. Improvement in high load ethanol-diesel dual-fuel combustion by Miller cycle and charge air cooling. Applied Energy 2018;210:138-51.

[36]   ANSYS FLUENT User's Guide 12.0. *Using Flow Boundary Conditions.* 2009.

[37]   Karlsson J. Förpackning av keramiska substrat. 2008.

[38]   Dimitrakopoulos N, Tunér M. Evaluation of engine efficiency, emissions and load range of a PPC concept engine, with higher octane and alkylate gasoline. Fuel 2020;275:117955.

[39]   Klaewkla R, Arend M, Hoelderich WF. A review of mass transfer controlling the reaction rate in heterogeneous catalytic systems. INTECH Open Access Publisher Rijeka; 2011.

[40]   Bennett CJ, Hayes RE, Kolaczkowski ST, Thomas WJ. An Experimental and Theoretical Study of a Catalytic Monolith to Control Automobile Exhaust Emissions. Proceedings: Mathematical and Physical Sciences 1992;439(1907):465-83.

[41]   Joshi SY, Harold MP, Balakotaiah V. Overall mass transfer coefficients and controlling regimes in catalytic monoliths. Chemical Engineering Science 2010;65(5):1729-47.

[42]   Lee JH, Trimm DL. Catalytic combustion of methane. Fuel Processing Technology 1995;42(2):339-59.

[43]   Deutschmann O. Modeling of the Interactions Between Catalytic Surfaces and Gas-Phase. Catalysis Letters 2015;145(1):272-89.